Hindawi
Wireless Communications and Mobile Computing
Volume 2018, Article ID 9656029, 10 pages
https://doi.org/10.1155/2018/9656029

Research Article

Spatiotemporal Statistical Channel Model for Indoor Corridor at 14 GHz, 18 GHz, and 22 GHz Bands

Nicholas O. Oyie and Thomas J. O. Afullo

Discipline of Electrical, Electronic and Computer Engineering, Howard College Campus, University of KwaZulu-Natal, Durban 4041, South Africa

Correspondence should be addressed to Nicholas O. Oyie; 217063428@stu.ukzn.ac.za

Received 9 August 2018; Revised 26 October 2018; Accepted 21 November 2018; Published 9 December 2018

Guest Editor: Ernest Kurniawan

Several techniques have been proposed to overcome challenges of meeting demands for higher data rates in wireless communication. Space-time diversity method is proposed to exploit spatiotemporal nature of the channel; hence, a comprehensive knowledge of the spatiotemporal properties of a channel is required. In this paper, a measurement-based channel model that considers both delay and angular domains of an indoor corridor channel for 14 GHz, 18 GHz, and 22 GHz is proposed. A nonparametric Gaussian kernel density estimation method is applied for cluster identification for the three frequency bands. This work proposes a spatiotemporal model that conditions the model parameters on the azimuthal spatial domain. The clusters are modeled on the complete azimuth plane and a Gaussian estimation distribution is fitted onto the empirical data plot. Both clusters and multipath components are modeled and results are compared with Saleh-Valenzuela model parameter values. The results show that both clusters and multipath components can be estimated by probability density functions that follow Gaussian and Laplacian fits on the spatial domain for indoor corridor environment, respectively.

1. Introduction

The challenges of spectrum shortage can be overcome by putting in place efficient and reliable wireless communication channel models. The frequency bands above 6 GHz promise large bandwidths and are thus desirable for application in fifth generation (5G) networks and beyond [1]. For optimum wireless communication systems' operation, massive multiple-input-multiple-output (MIMO) techniques have been introduced with capabilities to exploit both delay and angular domains to maximize capacity [2]. A successful design and deployment of indoor environment systems such as Femto Access Points, relies on an in-depth knowledge of radio channel propagation in terms of spatiotemporal channel fading [3].

Many studies have considered both spatial and temporal correlation properties of a propagation channel [3–5]. The space-time processing techniques' performance is dependent on efficient modeling of the correlation between spatial and temporal domains of propagation at a particular frequency band. Based on channel measurements, the Saleh-Valenzuela (S-V) model is one of the popular and widely used models that describe the stochastic properties of path time of arrival (ToA) and amplitudes of the resolvable multipath components (MPCs) in a wireless communication system. It assumes the Poisson process in modeling both MPCs' and clusters' ToA [6]. This model was used as the basis for the IEEE 802.15.3a model and is also used to compare standardization proposals for wireless personal area networks (PANs) [7].

An extension of S-V model (ES-V) was introduced which captured both temporal and angular information [8–10] for low-data speed wireless PANs. It assumes independence of spatial and temporal domains of each other. In addition, stochastic radio channel model (SRCM) based on measurement data [11] was conducted at 24 GHz frequency band in an office environment under line-of-sight (LOS) and non-line-of-sight (NLOS) scenarios. However, these models did not address the correlation of spatial and temporal properties of the channel, which are necessary for exploitation

of space-time techniques in signal processing. In [12], a measurement-based double-directional model for 60 GHz MIMO channel in a conference room was presented. The authors proposed a spatiotemporal channel model. Two approaches were provided for modeling spatiotemporal properties at 60 GHz band, namely, stochastic and ray-tracing (semideterministic approach).

More recently, the rotated directional antenna (RDA) and the uniform virtual array (UVA) approaches were adopted in investigation of a 60 GHz indoor office wireless channel in three dimensional (3-D) space [13]. The study considered the azimuth and the corresponding elevation domains simultaneously. Generally, the modeling was based on the ES-V model with specific emphasis on angular domain. However, these approaches did not incorporate the spatiotemporal correlation with parameters conditioned on the spatial domain in indoor corridor environments. Other studies on millimeter wave channel characterization can be found in [14–19].

The contribution of this paper is threefold: first, to have an in-depth study of statistical propagation channel characterization of the 14 GHz, 18 GHz, and 22 GHz bands in an indoor environment. In particular, it seeks to study the clustering of MPCs and spatial and temporal correlation characteristics of an indoor corridor channel. Second, to propose a spatiotemporal model that incorporates correlation properties and clustering with parameter conditioning on the spatial domain. Finally, this paper describes the impact of structural design, construction materials, and general geometry of radio wave propagation channel in the indoor environment on the propagation characteristics at 14 GHz, 18 GHz, and 22 GHz. The intercluster (cluster distribution) and intracluster (MPC distribution) channel parameters and correlation properties are analyzed using two joint probability functions (pdfs).

The rest of this paper is organized as follows: Section 2 presents the channel measurement set up, environment, and cluster identification. A kernel density estimate (KDE) approach is described in this section. In Section 3, spatiotemporal model that assumes dependence in delay and spatial domains is described. The proposed model is presented under characterization of channel parameters in Section 4. Validation of the proposed channel model and conclusion are given in Sections 5 and 6, respectively.

2. Channel Measurements and Data Processing

2.1. Measurement Environment. The measurement campaign was performed in an indoor corridor environment of the 5^{th} floor of the Discipline of Electrical, Electronic and Computer Engineering building, University of Kwa-Zulu Natal, South Africa. The structural and construction materials of the corridor are made up of concrete and brick walls, tiled floor, plasterboard ceiling, and wooden doors to offices as depicted in Figure 1. The corridor is terminated by wooden doors on both ends and has a volume of $30 \times 1.4 \times 2.7$ m^3. Measurements were conducted with no movements of people in the corridor and doors remained closed. The corridor acted as a waveguide through which the waves were propagated from the Tx to the Rx via the direct path and the reflected or guided paths. Several scatterers (i.e., walls, floor, ceiling, lumps, doors, etc.) were in the vicinity of the Tx and the Rx that generated MPCs. The spatiotemporal correlation was analyzed in terms of the intercluster and intracluster parameters. The correlation between the spatial and temporal aspects of the propagation indoor corridor channel was modeled with the parameter values conditioned on the spatial domain for all the studied frequency bands.

2.2. Measurement Set Up. Channel measurements were done using a radio frequency signal generator (Rohde and Schwarz SMF 100A) and signal analyzer with a frequency range from 20 Hz to 40 GHz and maximum analysis bandwidth of 120 MHz (Rohde and Schwarz FSIQ 40) at the Tx and the Rx sides, respectively. A trigger signal was used to synchronize the Tx and the Rx systems during measurements. A pair of wideband vertically polarized (V-V) directional horn antennas with dBi gain of 19.5, half power beamwidth of 19.2° in elevation, and 18.4° in azimuth for 14 GHz were used as illustrated in Figure 2. At the frequency band of 18 GHz, the antenna gain, half power beamwidth elevation, and azimuth were 20.95 dBi, 15.6°, and 15.4°, respectively; while at 22 GHz, the antenna gain was 22.1 dBi and half power beamwidth was 13° in elevation and 15° in azimuth [20].

The Tx was fixed at one end of the corridor while the Rx was place at 1 m, 4 m, 8 m, and 12 m separations from the Tx for all the measurements at each frequency band on a LOS scenario as illustrated in Figure 1. Both the Tx and the Rx antennas were fixed at 1.6 m above the floor for measurements in all the frequency bands. The receiving horn antenna was rotated on the azimuth plane in steps of 30° from 0° (boresight angle). Consequently, the direct and the reflected rays were captured both on spatial and temporal domains to describe the characteristics of the propagation channel. The elevation angle of both the Tx and the Rx horn antennas was kept at 0° for all the measurement points. The highly directional Tx and Rx antennas and geometry of the measurement environment realized very low signal levels reflected from the ceiling and floor in this research. The ceiling and floor distances were further from transmitting and receiving antennas as compared to side walls.

2.3. Cluster Identification. Measurements were performed in the time domain with the Rx antenna rotated on the azimuthal plane to capture the properties of the spatial domain of the channel. A cluster is defined in this paper as MPCs with similar characteristics on the spatial and temporal domains. Several researchers have reported diverse definitions of a cluster [21–23]. The MPCs resulted from reflections from scatterers along the propagation channel, a phenomenon previously reported in [6]. A number of parametric clustering techniques have been proposed such as K-means and Fuzzy C-means clustering methods [13, 24, 25]. However, we used the KDE technique which is a nonparametric density estimation procedure [26]. This technique was used in the identification of clusters from the measurements data. The KDE technique is appealing as it is

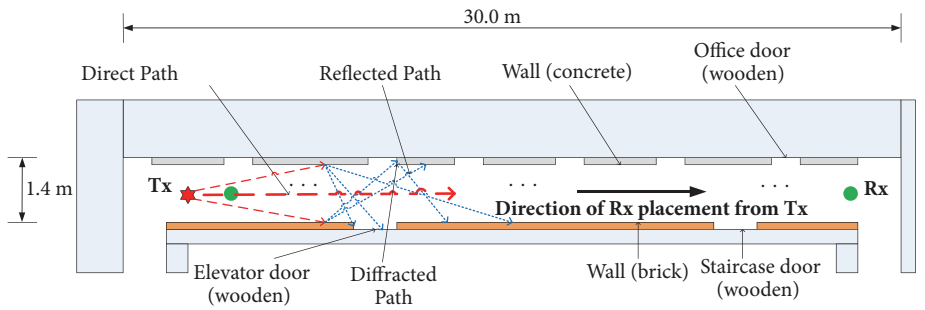

Figure 1: Indoor corridor floor layout.

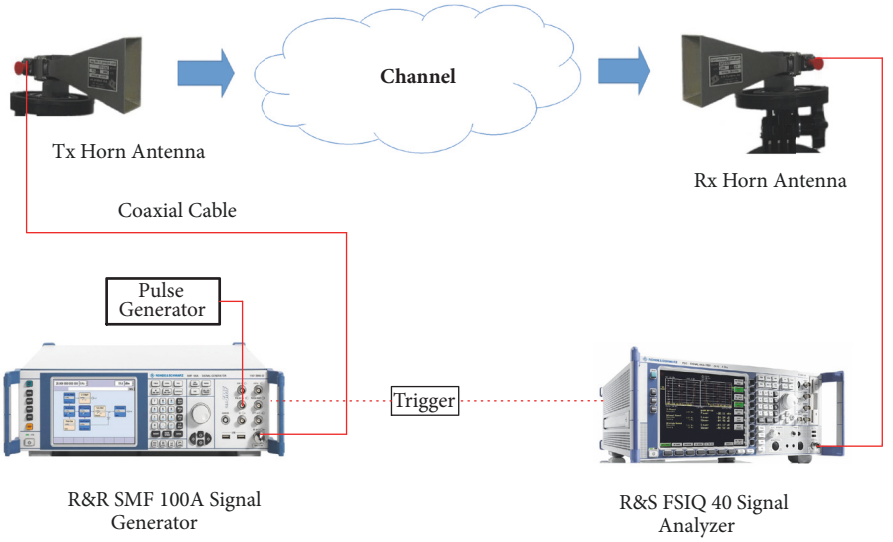

Figure 2: Measurement equipment.

solely based on the sample and hence avoids specification of the wrong parametric family as much as possible with the parametric approaches [27].

A joint delay and angular clustering method such as KDE has been used in [3] to make identification of multipath clusters more realistic and practical. Recently, authors in [28] proposed a new algorithm for clustering measurement data based on KDE. In this paper, a Gaussian KDE is proposed to estimate the MPCs clusters in an indoor environment. We conducted measurements using a custom-made channel sounder and the applied estimation method fairly clustered the MPCs in both time and angular domains. The data set of our measurements has two components: spatial and temporal domains. We applied a two-dimensional (2-D) kernel analysis directly as it is often easier to visualize densities in 2-D [26]. The KDE for a 2-D data set can be expressed as in (1):

$$\hat{f}(t,\Theta) = \frac{1}{nh_t h_\Theta}\sum_{i=1}^{n} K_t\left(\frac{t-t_i}{h_t}\right)\cdot K_\Theta\left(\frac{\Theta-\Theta_i}{h_\Theta}\right) \quad (1)$$

where h_Θ and $K_\Theta(\cdot)$, and h_t and $K_t(\cdot)$ are bandwidths and kernel functions of spatial and temporal domains, respectively, and n is the number of observations of measurement data for $t, \Theta \in \Re$. We applied a Gaussian KDE technique on the 2-D data set because of its robustness, simplicity, and convenience [3, 29] as expressed in (2) and (3) for time and angular domains, respectively:

$$K_t\left(\frac{t-t_i}{h_t}\right) = \frac{1}{\sqrt{2\pi}}\exp\left(-\frac{(t-t_i)^2}{2h_t^2}\right) \quad (2)$$

$$K_\Theta\left(\frac{\Theta-\Theta_i}{h_\Theta}\right) = \frac{1}{\sqrt{2\pi}}\exp\left(-\frac{(\Theta-\Theta_i)^2}{2h_\Theta^2}\right) \quad (3)$$

Optimal bandwidth was automatically chosen without a compromise between under- or oversmoothing [26]. Figures 3, 4, and 5 show the spatiotemporal MPCs contour plots of the measurement data for the three frequency bands. From the plots, it is clearly observable that MPC clusters exist in both space and time domains. For instance, a scatter plot is shown in Figure 6 for 22 GHz MPCs received in the

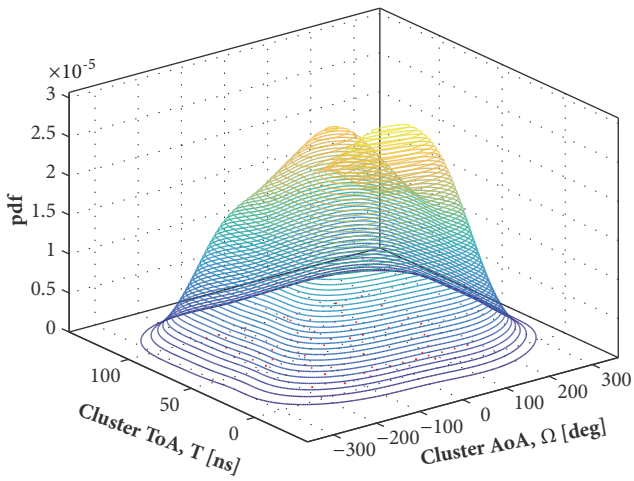

Figure 3: MPCs AoA-ToA contour plot for 14 GHz.

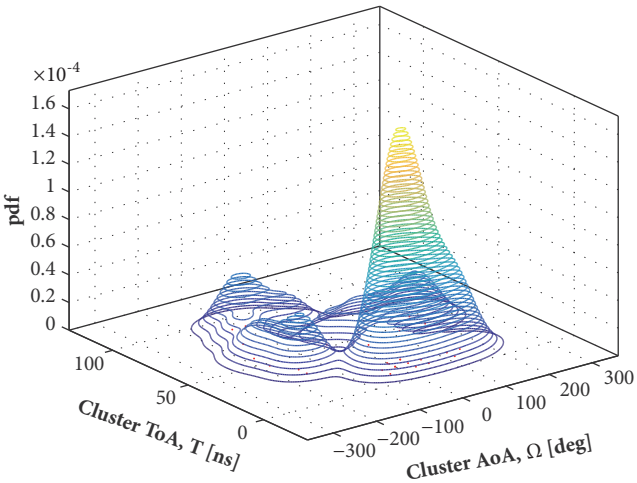

Figure 4: MPCs AoA-ToA contour plot for 18 GHz.

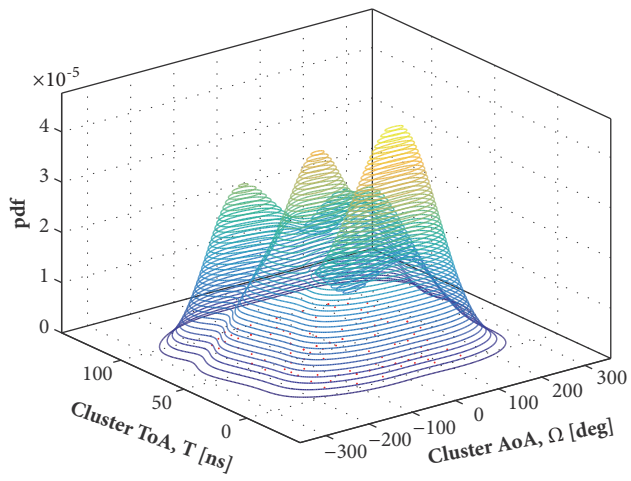

Figure 5: MPCs AoA-ToA contour plot for 22 GHz.

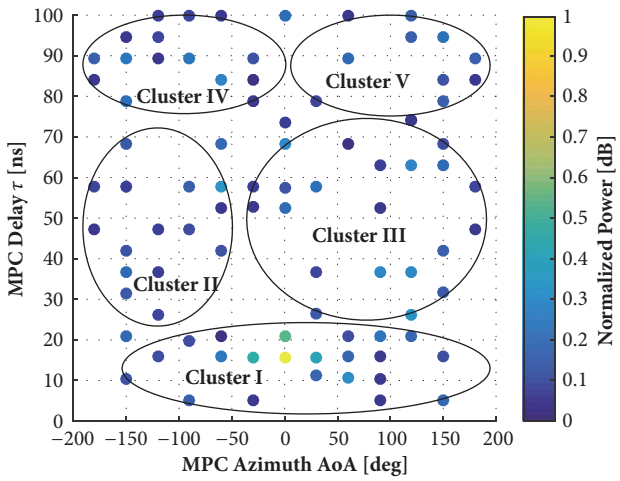

Figure 6: Scatter plot of MPCs for 22 GHz.

corridor indicating the location in space and time where the estimated clusters were positioned. After the 2-D Gaussian KDE processing, the clusters were singled out by visual inspection. Other works that employed visual inspection to identify clusters are [3, 6, 10].

3. Spatiotemporal Statistical Model

As reported in the S-V model, multipath components arrive at the receiver in clusters with delayed time of arrival and attenuated amplitudes [6]. The MPCs are reflected rays from scatterers that act as image sources along the propagation path. In an indoor corridor environment, these scatterers are generally the internal side walls, floor, ceiling, staircase, lamps, doors, and windows. Measurement data has thus been used to statistically characterize and model the indoor propagation channel such as S-V model.

The model presents parameters that can be used in simulation of the channel for in-depth understanding of the propagation phenomenon of the indoor corridor environment. The ES-V model is widely used and is based on clusters to derive channel parameters with the impulse response given by (4) [12]:

$$h(t,\Theta) = \sum_{m=0}^{M}\sum_{n=0}^{N_m}\beta_{n,m}e^{j\chi_{n,m}}\delta\left(t - T_m - \tau_{n,m}\right) \cdots \delta\left(\Theta - \Omega_m - \omega_{n,m}\right) \quad (4)$$

where h is the channel response and $\beta_{n,m}$ is the complex amplitude of the nth MPC in the mth cluster. T_m and Ω_m are the ToA and angle of arrival (AoA) of the mth cluster, respectively; $\tau_{n,m}$ and $\omega_{n,m}$ are the ToA and AoA of the nth ray (i.e., MPC) in the mth cluster, respectively; $\chi_{n,m}$ is the phase of each MPC; and $\delta(\cdot)$ is the Dirac delta function. $\chi_{n,m}$ is assumed to randomly and uniformly vary over $[0,2\pi)$. The

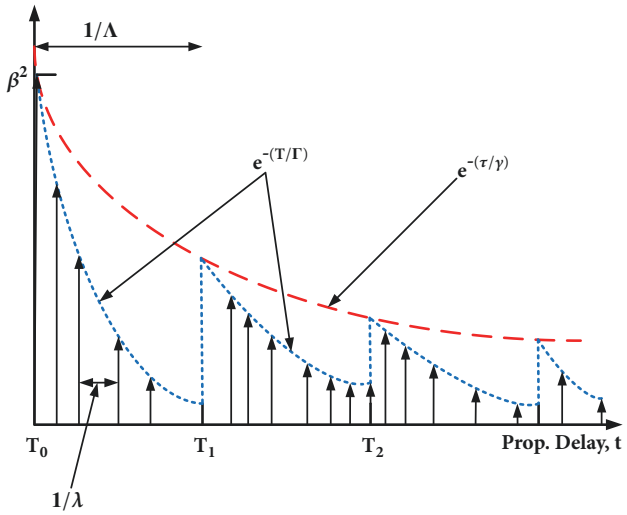

Figure 7: S-V mode for indoor multipath propagation.

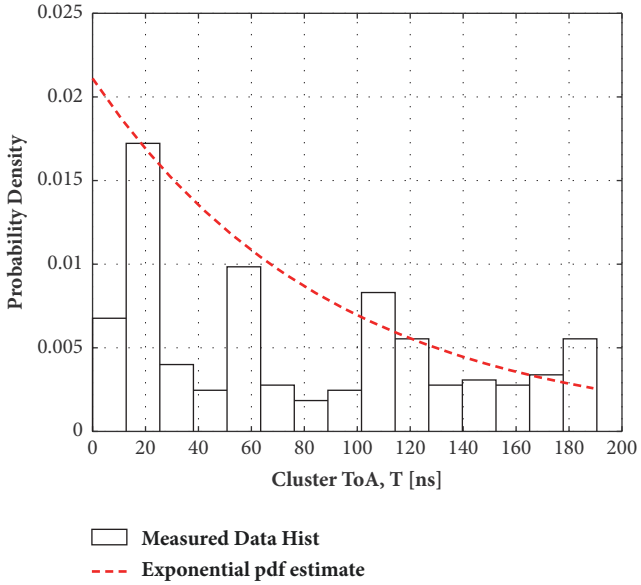

Figure 8: Marginal ToA pdf for clusters at 18 GHz.

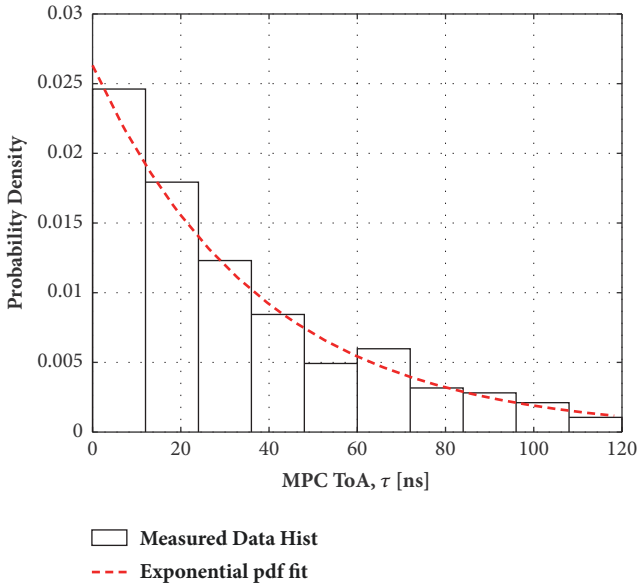

Figure 9: Intercluster marginal ToA pdf for MPCs at 22 GHz.

mean- squared power of the nth ray in the mth cluster is given by (5) and (6) [12] and depicted in Figure 7:

$$\overline{\beta_{n,m}^2} = \overline{\beta^2\left(T_m, \tau_{n,m}\right)} \tag{5}$$

$$= \overline{\beta^2\left(0,0\right)} e^{-T_m/\Gamma} e^{-\tau_{n,m}/\gamma} \tag{6}$$

where the cluster and ray ToA decay constants are represented by Γ and γ, respectively. $\overline{\beta^2(0,0)}$ is the average power of the first ray of the first cluster [10]. The cluster and ray arrival times can be described by two Poisson processes if delay and angular properties are modeled independently. The interarrival time of clusters can be characterized by an exponential probability density function as presented in Figure 8 for the 18 GHz band. In addition, ray interarrival times within each cluster can be independently described in the same manner as shown by histogram plot in Figure 9. Consequently, each cluster's arrival time is estimated by a distributed random variable that decays exponentially and is conditioned on the arrival of the previous cluster. The distributions of cluster and ray arrival rates, assumed independence, can be expressed as in (7) and (8), respectively [12]:

$$p\left(T_m \mid T_{m-1}\right) = \Lambda e^{-\Lambda\left(T_m - T_{m-1}\right)}, \quad m > 0 \tag{7}$$

$$p\left(\tau_{n,m} \mid \tau_{n-1,m}\right) = \lambda e^{-\lambda\left(\tau_{n,m} - \tau_{n-1,m}\right)}, \quad m > 0 \tag{8}$$

where Λ is the cluster interarrival rate and λ is the ray arrival rate (see Figure 7).

It is worth noting that the ES-V model assumes that time and angular parameters can be modeled independently. However this work jointly model the delay and spatial domain characteristics using a conditional angular-delay distribution function [3, 12].

4. Characterization of the Channel Parameters

In this section, we characterize the propagation channel in terms of intercluster and intracluster parameters. A statistical characterization of the behavior of these parameters may be carried out by fitting the measurement data against the proposed theoretical distributions. The estimated intercluster and intracluster parameters results are presented and compared with S-V model values discussed in Section 3. As stated earlier, three frequency bands are considered in an indoor corridor environment (i.e., 14 GHz, 18 GHz, and 22 GHz) in LOS scenario and the average number of clusters for the 14 GHz band on the angular domain represented by the histogram plot of Figure 10.

4.1. Intercluster Parameters. The correlation between temporal and angular domains is noted to generate a joint

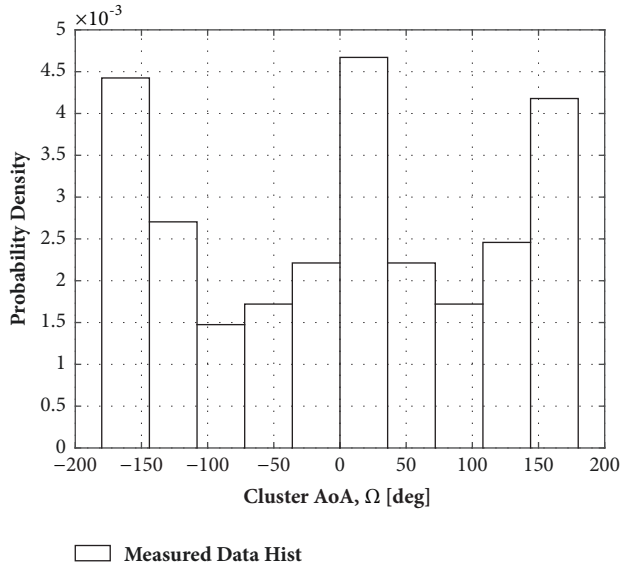

Figure 10: Average number of clusters at 14 GHz.

distribution of cluster-based model. The joint probability distribution function (pdf) of clustering $f(T_m, \Omega_m)$ is given by (9):

$$f\left(T_m, \Omega_m\right) = f\left(\Omega_m \mid T_m\right) \cdot f\left(T_m\right) \tag{9}$$

where $f(\Omega_m \mid T_m)$ is conditional AoA pdf for the cluster and $f(T_m)$ is the marginal ToA pdf for the cluster. We considered all possible AoAs for the received reflections in the indoor corridor to empirically determine the joint pdf. Different frequency bands were considered with Tx system placed at one end of the corridor while the Rx was successively placed at four different locations from the Tx and all possible AoAs captured. The received MPCs are modeled by the joint AoA pdfs for each of the frequency bands. Figures 3, 4, and 5 show the joint pdf, $f(T_m, \Omega_m)$ for the 14 GHz, 18 GHz, and 22 GHz cases, respectively. Figure 6 shows the scatter plot of the estimated clustered MPCs for 22 GHz. The clustering technique shows that there are five clusters of MPCs in the indoor corridor arriving at the Rx.

The angular axes for all the bands span the range -180° and +180° to form the 360° full spatial azimuth span. We noted significant differences in the statistical analysis of the spatiotemporal domains of the channel at varying frequencies. MPCs that arrive at the Rx with both short and long delays at 14 GHz (Figure 3) have a wider angular range and uniform amplitude with three distinct clusters. The three clusters are due to the direct path and the reflected MPCs from both side walls. The 18 GHz band has paths with restricted angular range for short delays while having highly attenuated longer delay paths that have relatively wide angular range. Four clusters are observed as shown in Figure 4. This could be attributed to the effects of the corridor geometry and structural design, resulting in destructive interference. In addition, surface roughness could have resulted in higher distortion and attenuation at this particular frequency band. This phenomenon needs further investigation by considering varying measurement environments. At 22 GHz band, five clusters were observed. The cluster with short delay paths has wider angular range than those with longer delays as seen in Figure 5. It is also notable that the signals are less attenuated as compared to 18 GHz although number of clusters increased. Received MPCs at the Rx over short delays are composed of the direct LOS path and/or reflections from structures in the vicinity of the Rx. The Rx placed in the corridor is surrounded by walls, doors, floor, and ceiling, thus the reflections come from a large angular range.

In Figure 4, for example, arrival paths with relatively short delay range have larger angular ranges and are observed to be reflected from both walls of the corridor. Arrival paths with larger delays are largely due to reflections from corridor end wall or multiple reflections within the corridor as radio waves are guided by the waveguide-like corridor. These paths of course suffer higher attenuation than early arrival ones because of longer paths traveled and multiple reflections. This characteristic of radio propagation in the channel is attributed to the general structure of the measurement environment (Figure 1). As expected, one observes that different frequency bands have different propagation characteristics in the same environment. The probability of path arrivals is highest at 0° and for the shorter delay ranges in all the frequency bands. In addition, larger delay paths have high probability at 180° due to corridor end wall reflections as shown in Figures 3, 4, and 5. Paths arriving from side walls incur least probabilities and are most attenuated. This is partly due to the geometry, structural design, and construction materials of the corridor. The cluster ToA has been modeled by the Poisson process that assumes independence of arrivals [6, 10]. However, in a regular structural design, such as indoor corridors, this independence does not hold [3]. In this paper, a nonparametric estimation of the pdf is used to model the arrivals based on measurement data. This is a more general approach with no *a priori* assumption of Poisson process satisfied by the cluster arrival times.

The empirical cluster AoA histogram density for 14 GHz is shown in Figure 10. The 14 GHz and 22 GHz frequency bands have a similar channel clusters behavior. Estimation of a cluster's marginal ToA pdf $f(T_m)$ was done by accumulation of all the AoAs, $\{\Omega_m\}_m \in M$ for 18 GHz as presented in Figure 8. The estimated pdf is plotted as the dotted curve and the $f(T_m)$ is modeled by an exponential pdf expressed as in (10):

$$f\left(T_m\right) = \begin{cases} \dfrac{1}{\mu_T} \exp\left(\dfrac{T_m}{\mu_T}\right), & T_m > 0 \\ 0, & \text{otherwise} \end{cases} \tag{10}$$

where μ_T is the mean ToA.

The cluster joint AoA pdfs for 14 GHz, 18 GHz, and 22 GHz are estimated using this new technique. $f(\Omega_m \mid T_m)$ is characterized by an empirical distribution that fits the data. We considered the azimuthal spatial range from -180° to 180°. The cluster joint AoA pdf is further estimated using a Gaussian pdf as the mean and standard deviation values are determined. We observed low probability density values for clusters with arrival paths with longer delays. Figures

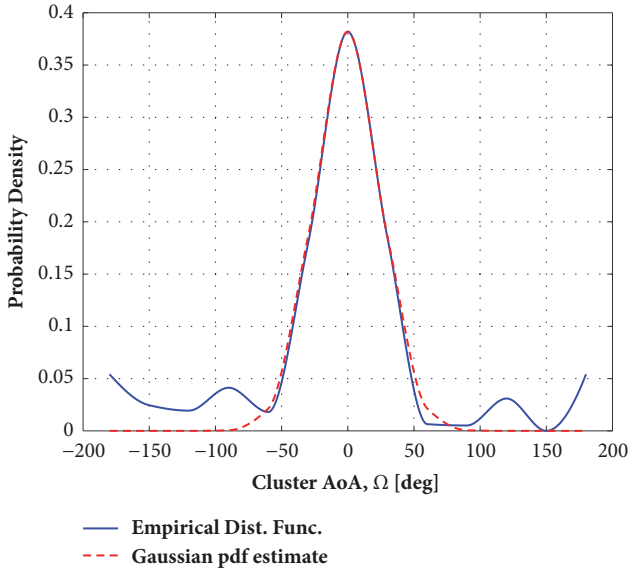

Figure 11: Cluster azimuth AoA pdf for 14 GHz.

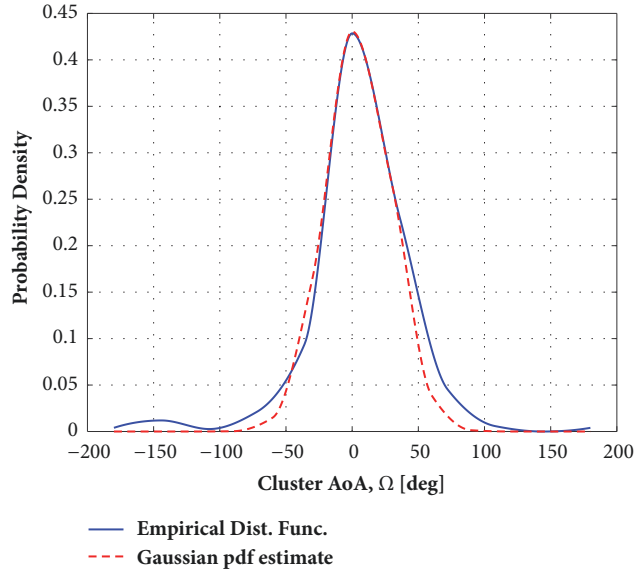

Figure 12: Cluster azimuth AoA pdf for 18 GHz.

11, 12, and 13 show the plots of the empirical distribution function and the estimated Gaussian pdfs. From the graphs, it is observed that a Gaussian pdf can closely estimate the cluster AoA in an indoor corridor at 14 GHz, 18 GHz, and 22 GHz frequency bands. The proposed Gaussian pdf to model the channel is given by (11):

$$f\left(\Omega_m, T_m\right) = \frac{1}{\sqrt{2\pi}\cdot\sigma_{\Omega_m}} \exp\left\{-\frac{\Omega_m^2}{2\sigma_{\Omega_m}^2}\right\} \tag{11}$$

where σ_{Ω_m} is the standard deviation conditioned upon Ω_m. However, the tails of the empirical distributions for 14 GHz and 22 GHz have pronounced clusters appearing between 90° and 180° and -90° and -180°. This may be due to the presence of strong MPCs received as reflected, scattered, and diffracted from back and side walls. The approximation errors at these spatial ranges are within the acceptable margin as the probability of occurrence in most cases is less than 0.08. For 18 GHz, the empirical values are approximated better as weaker and fewer MPCs were received from the back and side walls. This may be due to the impact of structural design and construction materials of the corridor at this propagation wavelength.

4.2. Intracluster Parameters. The ToA of the MPCs have been modeled by the Poisson process. In this approach, each cluster consists of a number of MPCs. To identify an individual ray composing a cluster, experimental measurements should be done in both spatial and temporal domains [30]. An extension of the proposed nonparametric projection of the pdf of the arrival time of clusters based on the measured data is adopted. The MPC marginal ToA pdf $f(\tau_{n,m})$, is estimated using the accumulated MPCs' AoAs, $\{\omega_n\}_{n\in N}$. Figure 9 shows the MPC marginal ToA histogram probability density for 22 GHz, with the number of MPCs estimated by an exponential pdf plotted in dotted curve. The observed results are in

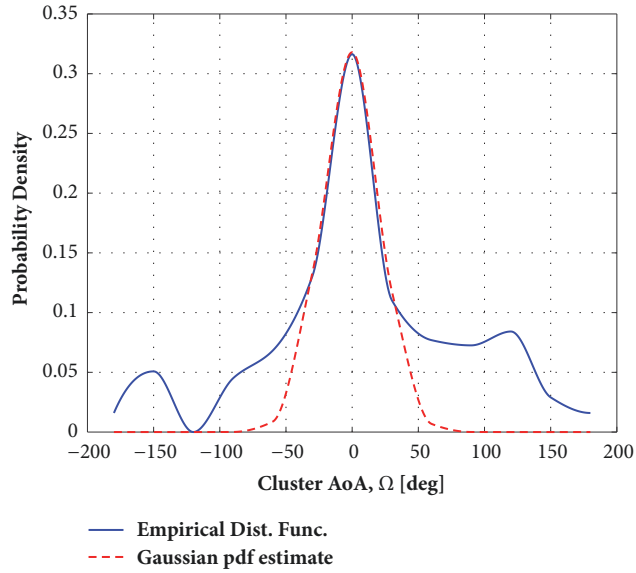

Figure 13: Cluster azimuth AoA pdf for 22 GHz.

agreement with [3, 31]. The joint MPCs position per cluster $f(\tau_{n,m}, \omega_{n,m})$ can be expressed as (12):

$$f\left(\tau_{n,m}, \omega_{n,m}\right) = f\left(\omega_{n,m} \mid \tau_{n,m}\right) \cdot f\left(\tau_{n,m}\right) \tag{12}$$

where $f(\omega_{n,m})$ is the MPC azimuth AoA pdf, expressed as a zero-mean Laplacian pdf in (13)

$$f\left(\omega_{n,m}, \tau_{n,m}\right) = \frac{1}{\sqrt{2\sigma_\omega}} \exp\left(-\sqrt{2}\frac{\left|\omega_{n,m}\right|}{\sigma_\omega}\right) \tag{13}$$

where σ_ω is the standard deviation conditioned on the spatial domain for $\tau_{n,m}$. Figure 14 shows a scatter plot of the MPCs' AoA with respect to ToA while considering the MPCs' normalized power. The result shows that there is a correlation

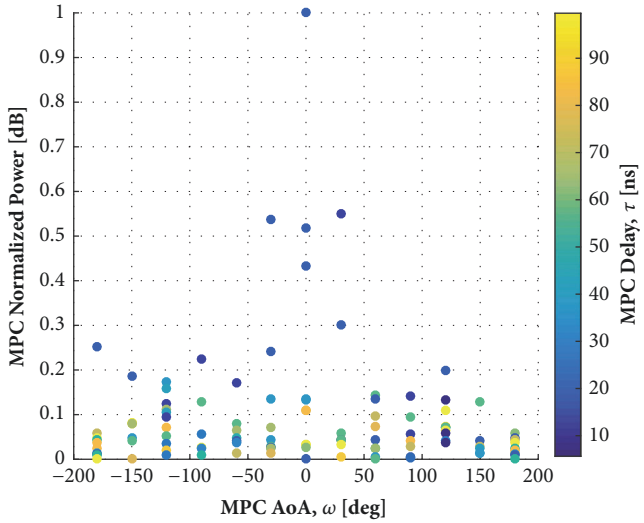

Figure 14: MPCs scatter plot of marginal AoA for 14 GHz.

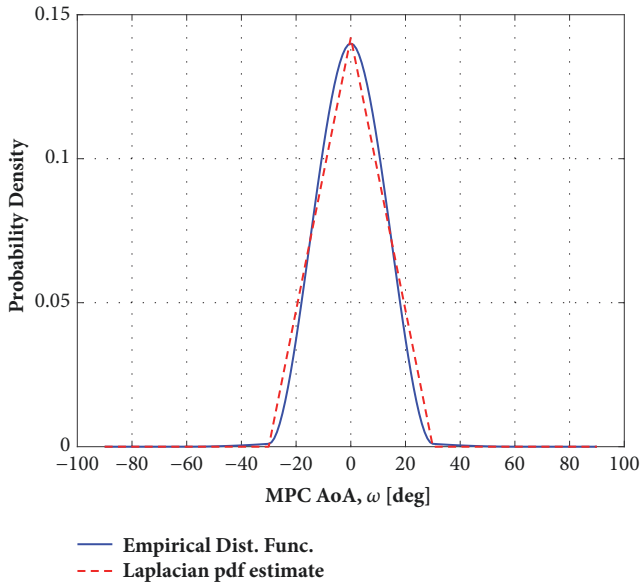

Figure 15: Intracluster azimuth AoA pdf for MPCs for 14 GHz.

between AoA and ToA with respect to power. The paths with shortest delays arrive at 0° with highest power. Paths with larger delays have much wider spatial range and lower power at the Rx. The delayed MPCs are attenuated on the side walls of the corridor as they travel along the corridor. This implies that the probability density of MPC's AoA is a joint distribution of time and angle of arrival, as indicated in (12).

Previous research has reported that the Laplacian distribution can be adopted to estimate the MPC's AoA pdf [3, 10, 11]. However, no justifiable reason is given over this choice except for it is fitting well against measured data. In [3], the effects of local and distant scatterers on the distribution of MPC's AoA at the Rx are illustrated. As can be seen in Figure 15, the scatters at the vicinity of the Rx can cause a large spatial range, and the Laplacian pdf neatly estimates the empirical distribution. The corridor, side walls, doors, ceiling, and floor can generate a lot of reflections in a wide spatial range. These paths are delayed and weak. However, distant scatterers tend to generate reflections within a narrow spatial range. The effect of distant scatterers was established to be at the spatial range of -30° to 30°. On assumption of same number of local and distant scatterers and each generating same number of MPCs, there would be a higher density on one direction and lower on the other. This gives a distribution similar to the Laplacian distribution with high density at the center and lower density on the side spatial areas.

5. Validation of the Proposed Channel Model

To validate the proposed pdf estimation of the indoor corridor channel at 14 GHz, 18 GHz, and 22 GHz frequency bands, the channel parameters are compared with S-V model. The estimated model and the S-V model channel parameters are listed in Table 1. The building used in [6] to conduct measurements is almost similar to our measurement environment. We extracted the model parameters based on LOS scenarios for all the frequency bands. The temporal parameters are estimated using the methods in [6] and are generally larger than the S-V model parameters. The greatest discrepancy is in the estimates for the value of Λ because more clusters were observed (3-5 clusters) in the indoor corridor as compared to 1-2 in [6]. This was due to the structural design, construction materials, and general geometry of the corridor. In addition, the frequency bands considered were much higher than that in S-V model. We were able to identify the clusters that overlap in time but separate in spatial domain. This clearly separated clusters that would have been identified as a single group in time domain only. The S-V model has no spatial parameters values. Both Γ and γ were observed to be fairly similar to S-V model for 18 GHz and slightly higher for other frequency bands.

6. Conclusion

The spatiotemporal characteristics of the channel were captured and this information was used for MPCs clustering using a 2-D Gaussian KDE technique. In addition, the intercluster and intracluster parameters were extracted and the correlation between time and angular domains in clustering was determined using the proposed channel model. For 14 GHz, three clusters were observed, with the main cluster being between -30° and 30°. The clusters emerging at the tails of the distributions were as a result of the corridor end wall reflections especially for 14 GHz and 22 GHz bands. The 18 GHz band has a smoother tail because of weak MPCs received from the end and side walls. The clusters' distributions were modeled based on the spatial domain irrespective of time of arrival with variation in mean angle for all the measurements. Rays with short delays made up the clusters between -90° and 90° for all the frequency bands. The MPCs' distribution within a cluster was approximated with a Laplacian pdf, with standard deviation from 3.0° to 3.3° for the three studied frequency bands.

Table 1: Intercluster and intracluster channel parameters for LOS 14 GHz, 18 GHz, and 22 GHz frequency bands.

Parameter	Notation	Units	14 GHz	18 GHz	22 GHz	S-V Model
Cluster rate of arrival	Λ	[1/ns]	0.05	0.04	0.05	0.003
Ray rate of arrival	λ	[1/ns]	0.2	0.5	0.2	0.2
Cluster rate of decay	Γ	[ns]	90	60	90	60
Ray rate of decay	γ	[ns]	38	25	35	20
Cluster AoA mean	Ω_m	[deg]	0	5	0	-
Cluster st. dev.	σ_{Ω_m}	[deg]	25	25	22	-
Ray AoA mean	ϕ	[deg]	1.0	1.0	1.0	-
Ray st. dev.	σ_ϕ	[deg]	3.2	3.3	3.0	-

The application of the presented model in indoor corridor and enclosed environments with Tx antenna fixed at height h_t and typical Rx antenna at height h_r is described. For any arbitrary distance between the Tx and the Rx antennas, the channel can be easily simulated based on the parameters given in Table 1. The channel can be realized by simulating the MPCs as a Laplacian distribution, then the clusters of the MPCs can be determined as a Gaussian distribution. The simulated channel can be effectively applied in design and deployment of signal processing techniques, network protocols, and massive MIMO for indoor and enclosed environments.

The novelty of this work is the introduction of joint pdf estimates that describe the stochastic properties of the channel with channel parameters conditioned on the spatial domain. Furthermore, it describes the correlation of the intercluster and intracluster spatiotemporal characteristics of the channel. The extracted channel parameters enable reproduction of the channel by computer simulation. The result of this work is applicable in any indoor corridor or enclosed environments with a waveguide-like structural design and concrete and wooden (doors) materials on walls, e.g., pedestrian underpass, tunnels connecting buildings, underground passageways, and through-pass corridors in malls. The corridor can have any cross sectional dimension and length.

Data Availability

The data used to support the findings of this study are available from the corresponding author upon request.

Conflicts of Interest

The authors declare that they have no conflicts of interest.

References

[1] M. Nasr-Esfahani and B. S. Ghahfarokhi, "Improving spectrum efficiency in self-organized femtocells using learning automata and fractional frequency reuse," *Annals of Telecommunications-Annales des Télécommunications*, vol. 72, no. 11-12, pp. 639–651, 2017.

[2] S. Sivakrishna and R. S. Yarrabothu, "Design and simulation of 5G massive MIMO kernel algorithm on SIMD vector processor," in *Proceedings of the Conference on Signal Processing and Communication Engineering Systems (SPACES '18)*, pp. 53–57, Vijayawada, India, January 2018.

[3] C.-C. Chong, C.-M. Tan, D. I. Laurenson, S. McLaughlin, M. A. Beach, and A. R. Nix, "A new statistical wideband spatio-temporal channel model for 5-GHz band WLAN systems," *IEEE Journal on Selected Areas in Communications*, vol. 21, no. 2, pp. 139–150, 2003.

[4] R. B. Ertel, P. Cardieri, K. W. Sowerby, T. S. Rappaport, and J. H. Reed, "Overview of spatial channel models for antenna array communication systems," *IEEE Personal Communications*, vol. 5, no. 1, pp. 10–22, 1998.

[5] U. Martin et al., "Model scenarios for direction-selective adaptive antennas in cellular mobile communication systems – scanning the literature," *Wireless Personal Communications*, vol. 11, no. 1, pp. 109–129, 1999.

[6] A. A. Saleh and R. A. Valenzuela, "A statistical model for indoor multipath propagation," *IEEE Journal on Selected Areas in Communications*, vol. 5, no. 2, pp. 128–137, 1987.

[7] A. Meijerink and A. F. Molisch, "On the physical interpretation of the Saleh-Valenzuela model and the definition of its power delay profiles," *IEEE Transactions on Antennas and Propagation*, vol. 62, no. 9, pp. 4780–4793, 2014.

[8] A. F. Molisch, D. Cassioli, and C.-C. Chong, "A comprehensive standardized model for ultrawideband propagation channels," *IEEE Transactions on Antennas and Propagation*, vol. 54, no. 11, pp. 3151–3166, 2006.

[9] A. F. Molisch et al., "IEEE 802.15.4a channel model," *Final Report*, 2004.

[10] Q. H. Spencer, B. D. Jeffs, M. A. Jensen, and A. L. Swindlehurst, "Modeling the statistical time and angle of arrival characteristics of an indoor multipath channel," *IEEE Journal on Selected Areas in Communications*, vol. 18, no. 3, pp. 347–360, 2000.

[11] R. Heddergott, U. Bernhard, and B. Fleury, "Stochastic radio channel model for advanced indoor mobile communication systems," in *Proceedings of the 8th International Symposium on Personal, Indoor and Mobile Radio Communications (PIMRC '97)*, vol. 1, pp. 140–144, Helsinki, Finland, 1997.

[12] C. Gustafson, K. Haneda, S. Wyne, and F. Tufvesson, "On mm-wave multipath clustering and channel modeling," *IEEE Transactions on Antennas and Propagation*, vol. 62, no. 3, pp. 1445–1455, 2014.

[13] X. Wu, C.-X. Wang, J. Sun et al., "60-GHz millimeter-wave channel measurements and modeling for indoor office environments," *IEEE Transactions on Antennas and Propagation*, vol. 65, no. 4, pp. 1912–1924, 2017.

[14] B. Ai et al., "On indoor millimeter wave massive MIMO channels: measurement and simulation," *IEEE Journal on Selected Areas in Communications*, vol. 35, no. 7, pp. 1678–1690, 2017.

[15] J. Huang, C.-X. Wang, R. Feng, J. Sun, W. Zhang, and Y. Yang, "Multi-Frequency mmWave Massive MIMO Channel Measurements and Characterization for 5G Wireless Communication Systems," *IEEE Journal on Selected Areas in Communications*, vol. 35, no. 7, pp. 1591–1605, 2017.

[16] Q. Wang, B. Ai, D. W. Matolak et al., "Spatial variation analysis for measured indoor massive MIMO channels," *IEEE Access*, vol. 5, pp. 20828–20840, 2017.

[17] C. Xu, J. Zhang, Q. Zheng, H. Yu, and L. Tian, "Measurement-based delay spread analysis of wideband massive MIMO system at 3.5 GHz," in *Proceedings of the IEEE International Conference on Computational Electromagnetics (ICCEM '17)*, pp. 246–248, Kumamoto, Japan, March 2017.

[18] J. Li, B. Ai, R. He et al., "Measurement-based characterizations of indoor massive MIMO channels at 2 GHz, 4 GHz, and 6 GHz frequency bands," in *Proceedings of the IEEE 83rd Vehicular Technology Conference (VTC Spring '16)*, pp. 1–5, Nanjing, China, May 2016.

[19] N. Czink, M. Herdin, H. Özcelik, and E. Bonek, "Number of multipath clusters in indoor MIMO propagation environments," *IEEE Electronics Letters*, vol. 40, no. 23, pp. 1498-1499, 2004.

[20] N. O. Oyie and T. J. O. Afullo, "Measurements and analysis of large-scale path loss model at 14 and 22 GHz in indoor corridor," *IEEE Access*, vol. 6, pp. 17205–17214, 2018.

[21] M. Toeltsch, J. Laurila, K. Kalliola, A. F. Molisch, P. Vainikainen, and E. Bonek Sr., "Statistical characterization of urban spatial radio channels," *IEEE Journal on Selected Areas in Communications*, vol. 20, no. 3, pp. 539–549, 2002.

[22] J. E. Dietert and B. Rembold, "Stochastic channel model for outdoor applications based on raytrace simulations," in *Proceedings of the Millennium Conference on Antennas and Propagation (AP '20)*, Davos, Switzerland, April 2000.

[23] M. Steinbauer, A. F. Molisch, and E. Bonek, "The double-directional radio channel," *IEEE Antennas and Propagation Magazine*, vol. 43, no. 4, pp. 51–63, 2001.

[24] K. J. Kim, J. Yue, R. A. Iltis, and J. D. Gibson, "A QRD-M/Kalman filter-based detection and channel estimation algorithm for MIMO-OFDM systems," *IEEE Transactions on Wireless Communications*, vol. 4, no. 2, pp. 710–721, 2005.

[25] K. Dasani and A. Shrotriya, "Channel estimation and data detection with fuzzy C-means based em approach in MIMO system," in *Proceedings of the 2nd International Conference on Computational Intelligence and Communication Technology (CICT '16)*, pp. 559–563, February 2016.

[26] W. N. Venables and B. D. Ripley, *Modern Applied Statistics with S-PLUS*, Springer Science & Business Media, New York, NY, USA, 4th edition, 2013.

[27] C. Heinz and B. Seeger, "Cluster kernels: Resource-aware kernel density estimators over streaming data," *IEEE Transactions on Knowledge and Data Engineering*, vol. 20, no. 7, pp. 880–893, 2008.

[28] L. C. Matioli, S. R. Santos, M. Kleina, and E. A. Leite, "A new algorithm for clustering based on kernel density estimation," *Journal of Applied Statistics*, vol. 45, no. 2, pp. 347–366, 2018.

[29] D. W. Scott, *Multivariate Density Estimation: Theory, Practice and Visualization*, John Wiley & Sons, New York, NY, USA, 1992.

[30] A. Maltsev, R. Maslennikov, A. Lomayev, A. Sevastyanov, and A. Khoryaev, "Statistical channel model for 60 GHz WLAN systems in conference room environment," *Radioengineering*, vol. 20, no. 2, pp. 409–422, 2011.

[31] P. F. M. Smulders and A. G. Wagemans, "A statistical model for the MM-wave indoor radio channel," in *Proceedings of the 3rd IEEE International Symposium on Personal, Indoor and Mobile Radio Communications*, pp. 303–307, Boston, MA, USA, 1992.